

Observation of the Shadows of the Moon and Sun Using the Pierre Auger Observatory at an Average Energy of 7×10^{17} eV

Katarína Šimková^{ab,*} for the Pierre Auger Collaboration^c

^a*Vrije Universiteit Brussel, Physics Department, Pleinlaan 2, 1050 Brussels, Belgium*

^b*Université Libre de Bruxelles, Physics Department, Boulevard du Triomphe 2, 1050 Brussels, Belgium*

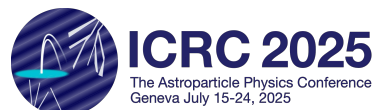
^c*Observatorio Pierre Auger, Av. San Martín Norte 304, 5613 Malargüe, Argentina*

Full author list: https://www.auger.org/archive/authors_icrc_2025.html

E-mail: spokespersons@auger.org

The interaction of cosmic rays with celestial bodies such as the Moon or the Sun produces a shadow in the arrival direction distribution of the cosmic rays reaching the Earth. Such deficits from an isotropic flux have been observed by astroparticle observatories below energies of 10^{15} eV. Above this energy, measurements were limited due to the low number of events as a result of the steeply falling cosmic-ray flux with energy. With more than 10.6 million events recorded during 20 years of operation of the Pierre Auger Observatory, we report the first observation of the shadow of the Moon at an average energy of 7×10^{17} eV with a maximum significance above 3σ . The shadow is an end-to-end check that the celestial directions are correctly reconstructed from the air shower data, and it is used here to derive the effective angular resolution for this dataset. Additionally, we present the results of a similar study on the shadow of the Sun.

39th International Cosmic Ray Conference (ICRC2025)
15–24 July 2025
Geneva, Switzerland



*Speaker

1. Introduction

The Moon and the Sun, as close-by celestial objects, remove cosmic rays from the approximately isotropic flux, creating shadows in the flux seen from Earth [1]. With a perfect observatory resolution, these shadows appear as disks with an angular radius of the Moon and the Sun, both approximately 0.26° on average. At TeV-PeV energies, the shape and location of the shadows are further distorted by deviations in the magnetic fields of the Sun and Earth, while at higher energies these effects are expected to be negligible [2, 3]. The final shape of the observed shadows is then influenced by the pointing and resolution of an observatory. That is why the shadows of the Moon and the Sun observed in TeV-PeV cosmic rays have been a commonly used technique to verify the performance of astroparticle observatories [3–8]. Because the flux of cosmic rays drops steeply with increasing energy, the observation above 10^{16} eV has not been possible until now. Using the large exposure of the Pierre Auger Observatory, we report the first observation of the shadows at an average energy of 7×10^{17} eV. In the last part of this proceeding, we use the shape of the deficit to evaluate the effective angular resolution as a combination of resolutions of events close to the Moon and Sun.

2. The Pierre Auger Observatory and the Data

The Pierre Auger Observatory, located in the southern hemisphere close to the city of Malargüe, in Argentina's Mendoza province, has been measuring extensive air showers (EASs) since 2004. It is composed of two key detectors. The first is the surface detector (SD) with a duty cycle of $\sim 100\%$ measuring the particles reaching the ground. The second is the fluorescence detector (FD), which measures the development of EAS in the atmosphere and provides an almost calorimetric energy estimate. The energy scale of SD is cross-calibrated with the FD measurements to obtain the energy for events measured by SD only [9].

The data used in this study come from the SD. Its main particle detector is a cylindrical water-Cherenkov detector (WCD) of 1.2 m height and 3.6 m diameter overlooked by three photomultipliers. During a recently-finished upgrade, the SD stations were further equipped by a Surface-Scintillator Detector (SSD) and a Radio Detector (RD), both placed on top of the WCD. The data in this study come from before the upgrade and consider signals from the WCDs only. The stations are placed on a triangular grid of regular spacing. Three arrays are defined according to the distances between the stations and their layout is shown in Fig. 1. The largest one, SD-1500, consists of 1600 WCDs with a spacing of 1500 m that span an area of 3000 km^2 measuring ultra-high-energy cosmic rays down to 10^{18} eV. The SD-750 is located within the SD-1500. It is composed of 61 stations with a spacing of 750 m and covers area of 27 km^2 . It is most sensitive to measure cosmic-ray primaries in the energy range between 10^{17} eV and 10^{18} eV. The last WCD array is SD-433 with 433 m spacing between 19 stations on 2 km^2 placed within SD-750. The SD-433 extends the sensitivity of the Observatory down to 10^{16} eV [10].

To obtain high-level variables such as arrival direction and the energy of a primary cosmic ray, the reconstruction of events is based on the same principle in all three arrays. At least three triggered WCDs are required to reconstruct the arrival direction based on the signal start time in each detector. The more WCDs that are used in the reconstruction, the more accurate is the

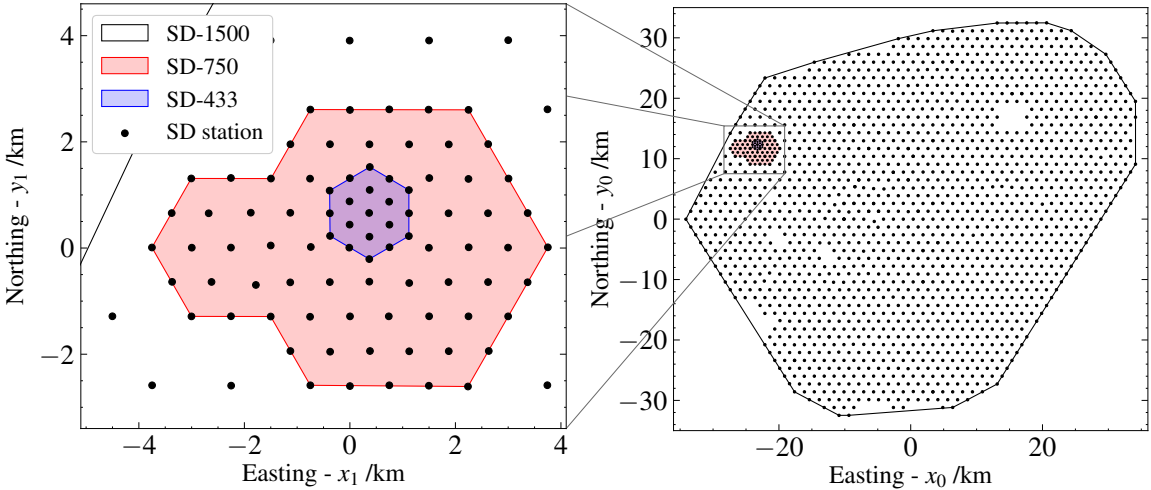


Figure 1: The layout of the SD-750 and SD-433 (red and blue region in the left panel) placed within the SD-1500 array (bounded by the black line in the right panel). The coordinates are centered at $(x_1, y_1) = (450627, 6113915)$ m and $(x_0, y_0) = (474255, 6102240)$ m.

reconstructed arrival direction. Previous studies, based on both measurements and simulations of SD-1500, estimated the angular resolution to be around 1° , improving to 0.4° with higher number of stations and energy [11].

In this study, we use 10.6 million events recorded by all three SD arrays between January 2004 and March 2023¹. The biggest contribution comes from SD-750 (64 % of the data), followed by SD-1500 (29 %) and SD-433 (7 %). Further, we select events that fall within 5° great-circle angular distance from the center of the Moon/Sun in local coordinates using the arrival direction of the event from the reconstruction and the position of the Moon/Sun from `Astropy` Python library [12]. This results in 18 215 events for the study of the lunar shadow and 18 650 events for the solar shadow.

3. The Relative Deficits due to the Moon and the Sun and their Significance

The flux in the direction of the Moon and Sun (on-region) is compared to an isotropic flux expectation. The isotropic expectation is deduced from generated sky regions that contain fake moons or suns (off-regions). Due to the fixed location of the Observatory and the 100% duty cycle of the SD, the exposure depends just on the declination (Dec) and it is uniform in right ascension (RA). We generate the off-regions using a time-shuffling method. By doing so, the time of an event is changed evenly 200 (100) times in ± 1 h (± 30 min) for the Moon (Sun)². The position of the events is changed in RA while its Dec remains the same. In local coordinates (Alt, Az) by changing the time, the Moon and the Sun move across the sky while for the event, Alt & Az are preserved. An example of the change of coordinates is shown in Fig. 2. With s off-regions (200 for the Moon and 100 for the Sun), the reference expectation is obtained as the average of the off-regions.

¹The time range is from the start of data-taking of each array (SD-1500: 2004, SD-750: 2008, SD-433: 2018) until the upgrade of the Observatory (AugerPrime).

²Using larger time interval for the Sun biases the off-region. Events close to the Sun are detected only during the day, which may introduce a dependence on RA.

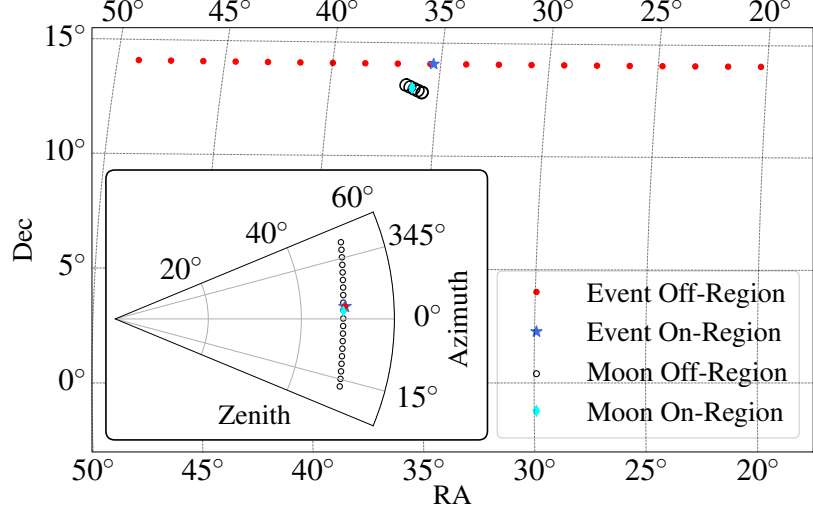
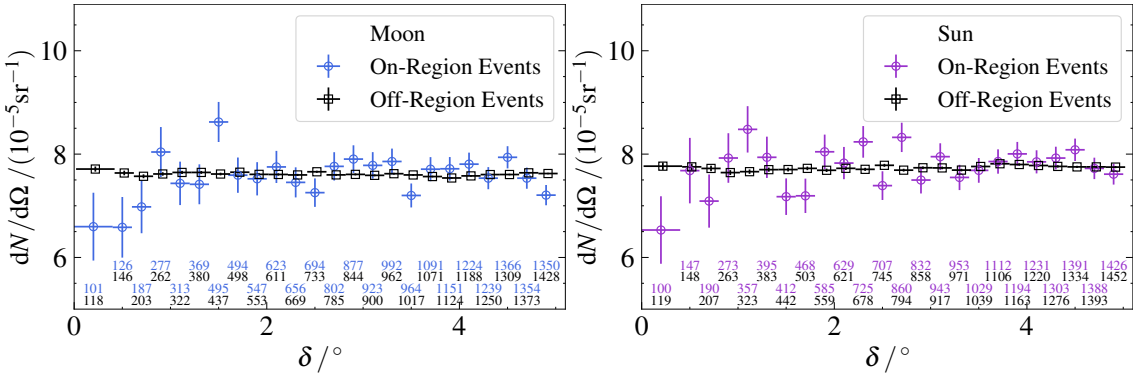


Figure 2: Example of the coordinate changes using the time shuffling method to generate the isotropic background estimate (average off-region), only every tenth off-region is shown. While the celestial object has approximately the same position in the equatorial coordinates, the off-events move in RA keeping the same declination which ensures the correct exposure estimate in the off-regions. In local coordinates, the position of the event is preserved while the fake moons move across the sky.



region and we sum the number of events below a certain angular distance δ . The relative difference is given by:

$$\Delta(\delta) = \frac{N_{\text{on}}(\delta)}{N_{\text{off}}(\delta)} - 1 \pm \sqrt{\frac{1}{N_{\text{on}}(\delta)} + \frac{1}{s N_{\text{off}}(\delta)}}. \quad (1)$$

These cumulative relative differences for the Moon and the Sun are shown in Fig. 4. Both exhibit a deficit below 1.4° confirming accurate pointing of the Observatory. The significance of the shadows is first calculated using the Li&Ma significance [13] and it is shown in Fig. 5. The maximum significance appears at $\delta = 0.85^\circ$ for both the Moon and the combined data, with values of 3.28σ and 3.36σ respectively. At this δ , the shadow of the Sun with the maximum significance of 2.41σ at $\delta = 0.23^\circ$, contributes only little to the combined significance.

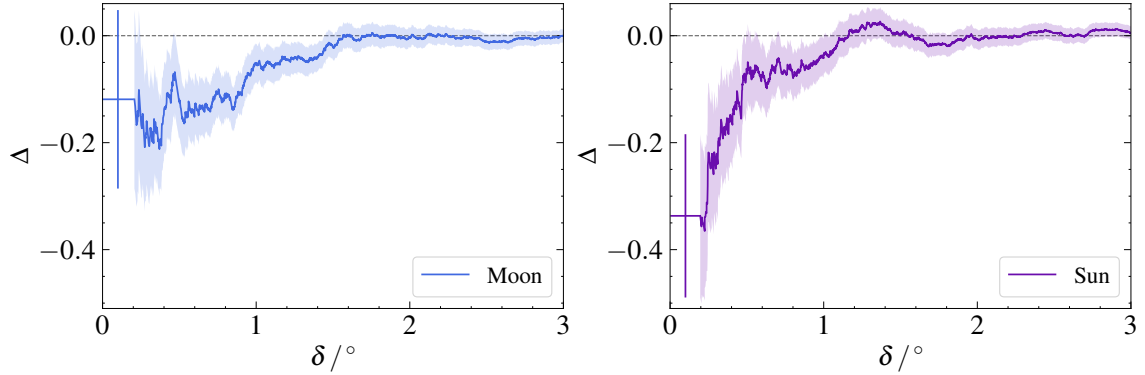


Figure 4: The relative difference of the cumulative number of events in the ‘on’ and ‘off’ regions as a function of the angular distance to the Moon (left panel) and to the Sun (right panel). Shaded bands indicate the 1σ statistical uncertainty. With the relative difference being cumulative, the individual data points are correlated.

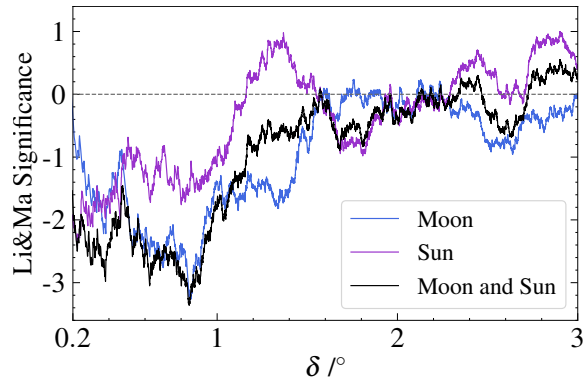


Figure 5: Individual and combined Li&Ma significances of the number of events close to the Moon/Sun compared to the isotropic expectation as a function of the angular distance between the events and the centers of the Moon/Sun.

4. The Effective Angular Resolution of the Observatory

As described in the introduction, the shape of the deficit is influenced by the resolution of the Observatory. The better the resolution, the fewer detected events migrate inside the shadow. Because the resolution improves with the multiplicity of stations participating in an event n , we divided the data set in samples based on the multiplicity. The deficit for these subsamples is illustrated in Fig. 6. We observe a decrease of Δ with increasing multiplicity, as expected when the angular resolution is improving. Due to the low statistics, the ordering is not very significant: At 0.5° , the deficit due to the Moon grows from $(12 \pm 7)\%$ for all the data, to $(26 \pm 13)\%$ with $n \geq 5$ and $(54 \pm 15)\%$ with $n \geq 6$. For the Sun the deficits at 0.5° are $(6 \pm 7)\%$ for all the data, $(28 \pm 13)\%$ for $n \geq 5$ and $(3 \pm 22)\%$ for $n \geq 6$.

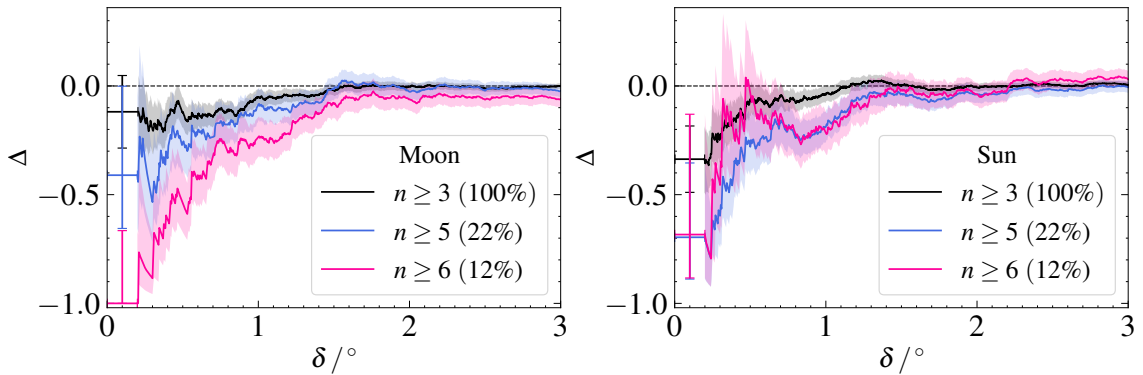


Figure 6: The relative difference of the cumulative number of events as a function of angular distance for events with different detector multiplicities n ; left panel: Moon, right panel: Sun. The fractions of the data samples compared to the full data set are quoted in the legend.

Next, we deduce the effective angular resolution of the Observatory based on the unbinned fit of the distribution of events around the center of the Moon and the Sun. The likelihood is constructed as in [4], where the shadowed events, dispersed by a 2-D Gaussian point spread function (PSF) are subtracted from the isotropic flux constant in $\cos \delta$. The number of events N in an infinitesimal annulus $d \cos \delta$ is given by:

$$\frac{dN}{d \cos \delta} = 1 - \int_0^{\delta_c} r' dr' \int_0^{2\pi} d\phi' \frac{1}{2\pi\sigma_r^2} \exp \left[-\frac{\xi(\cos \delta; r', \phi')^2}{2\sigma_r^2} \right]. \quad (2)$$

The integration goes over the disk of the Moon/Sun in polar coordinates (r', ϕ') with r' ranging from zero up to their angular radius $\delta_c = 0.26^\circ$. $\xi(\cos \delta; r', \phi')$ is the angular distance between an event and the infinitesimal element of the disk. The probability P is normalized to take into account that we consider only events up to $\delta = 5^\circ$:

$$P = \frac{dP/d \cos \delta}{\int_1^{\cos(5^\circ)} (dP/d \cos \delta) d \cos \delta} \quad \text{with} \quad \frac{dP}{d \cos \delta} = \frac{dN}{d \cos \delta} \frac{\int_1^{\cos(5^\circ)} d \cos \delta}{\int_1^{\cos(5^\circ)} (dN/d \cos \delta) d \cos \delta}. \quad (3)$$

The only free parameter in the fit is σ_r . We define the effective angular resolution of the Observatory as $\sigma_{68} = \sqrt{2.278}\sigma_r$ containing 68% probability of the 2-D Gaussian PSF. The result of the fit is

$\sigma_{68} = (0.61^{+0.21}_{-0.13})^\circ$ for the Moon data, $\sigma_{68} = (0.54^{+0.30}_{-0.15})^\circ$ for the Sun and $\sigma_{68} = (0.59^{+0.15}_{-0.11})^\circ$ for the combined data. The uncertainties are obtained from the shape of the likelihood and were further verified using a bootstrap of the data.

The significance of the fits (N_σ) can be evaluated using the likelihood ratio test as in [5] with no shadows (i.e. a very poor resolution) being the null hypothesis:

$$N_\sigma = \sqrt{2(w_{\max} - w_\infty)} . \quad (4)$$

Here w_{\max} is the log-likelihood of the best parameter value and w_∞ the log-likelihood of a poor resolution, we used $\sigma_r = 10^\circ$. The resulting significance of the fit of the Moon data $N_\sigma = 2.4$, for the Sun it is $N_\sigma = 1.8$, while for the combined data $N_\sigma = 3.0$.

The effective angular resolution represents the combination of multiple resolutions inherent to different multiplicities, zenith angles and the three arrays. Therefore, we performed a toy Monte-Carlo study to estimate the expected effective angular resolution based on the event-level resolutions assigned during the event reconstruction. The most probable value of the effective angular resolution of $(0.65 \pm 0.02)^\circ$ is consistent with all the three fit results, validating the event-level resolution estimates.

According to the σ_{68} of the fit of the shadow of the Moon, the maximum significance is expected at $\delta = (0.68^{+0.22}_{-0.14})^\circ$. This is consistent with the observed maximum of the Li&Ma significance at 0.85° (Fig. 5).

5. Conclusion

Analyzing more than 10.6 million events of the Pierre Auger Observatory above 10^{16} eV, we observe for the first time the shadow of the Moon and the Sun in such high-energy cosmic rays. The significance of the combined likelihood fit reaches 3σ . The contribution from the deficit of the Moon is larger, with a maximum Li&Ma significance of 3.28σ at 0.85° angular distance. The appearance of the deficit in our data validates the accurate pointing of the Observatory.

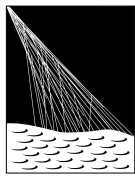
Based on the size of the shadow of the Moon, i.e. the likelihood fit, we find an effective angular resolution of $\sigma_{68} = (0.61^{+0.21}_{-0.13})^\circ$ for our Observatory. It represents a combination of resolutions varying in multiplicity, zenith angle and energy. With this resolution, the maximum significance of the shadows is expected at $\delta = (0.68^{+0.22}_{-0.14})^\circ$, which is consistent with our observation of the maximum Li&Ma significance at $\delta = 0.85^\circ$.

References

- [1] G.W. Clark, *Arrival directions of cosmic-ray air showers from the northern sky*, *Phys. Rev.* **108** (1957) 450.
- [2] Becker Tjus, J., Desiati, P., Döpper, N., Fichtner, H., Kleimann, J., Kroll, M. et al., *Cosmic-ray propagation around the Sun: investigating the influence of the solar magnetic field on the cosmic-ray Sun shadow*, *A&A* **633** (2020) A83.
- [3] IceCube collaboration, *Observation of the cosmic-ray shadow of the Moon with IceCube*, *Physical Review D* **89** (2014) .

- [4] THE CHICAGO AIR SHOWER ARRAY collaboration, *Observation of the shadows of the Moon and Sun using 100 TeV cosmic rays*, *Phys. Rev. D* **49** (1994) 1171.
- [5] D.E. Andreas et al., *Observation of shadowing of ultrahigh-energy cosmic rays by the Moon and the Sun*, *Phys. Rev. D* **43** (1991) 1735.
- [6] M. Amenomori et al., *Cosmic Ray Shadow by the Moon Observed with the Tibet Air Shower Array*, in *23rd International Cosmic Ray Conference (ICRC23), Volume 4*, D.A. Leahy, R.B. Hicks and D. Venkatesan, eds., vol. 4 of *International Cosmic Ray Conference*, p. 351, Jan., 1993.
- [7] P. Achard, O. Adriani, M. Aguilar-Benitez, M. van den Akker, J. Alcaraz, G. Alemanni et al., *Measurement of the shadowing of high-energy cosmic rays by the moon: A search for tev-energy antiprotons*, *Astroparticle Physics* **23** (2005) 411–434.
- [8] LHAASO collaboration, *The performances of the LHAASO-KM2A tested by the observation of cosmic-ray Moon shadow*, *PoS ICRC2021* (2021) 350.
- [9] THE PIERRE AUGER collaboration, *The Pierre Auger Cosmic Ray Observatory*, *Nuclear Instruments and Methods in Physics Research Section A: Accelerators, Spectrometers, Detectors and Associated Equipment* **798** (2015) 172.
- [10] THE PIERRE AUGER collaboration, *Performance of the 433 m surface array of the Pierre Auger Observatory*, *PoS ICRC2021* (2021) 224.
- [11] THE PIERRE AUGER collaboration, *Reconstruction of events recorded with the surface detector of the Pierre Auger Observatory*, *Journal of Instrumentation* **15** (2020) P10021.
- [12] Astropy Collaboration and Astropy Project Contributors, *The Astropy Project: Sustaining and Growing a Community-oriented Open-source Project and the Latest Major Release (v5.0) of the Core Package*, *Astrophysical Journal* **935** (2022) 167 [2206.14220].
- [13] T.P. Li and Y.Q. Ma, *Analysis methods for results in gamma-ray astronomy.*, *Astrophysical Journal* **272** (1983) 317.

The Pierre Auger Collaboration



PIERRE
AUGER
OBSERVATORY

- A. Abdul Halim¹³, P. Abreu⁷⁰, M. Aglietta^{53,51}, I. Allekotte¹, K. Almeida Cheminant^{78,77}, A. Almela^{7,12}, R. Aloisio^{44,45}, J. Alvarez-Muñiz⁷⁶, A. Ambrosone⁴⁴, J. Ammerman Yebra⁷⁶, G.A. Anastasi^{57,46}, L. Anchordoqui⁸³, B. Andrade⁷, L. Andrade Dourado^{44,45}, S. Andringa⁷⁰, L. Apollonio^{58,48}, C. Aramo⁴⁹, E. Arnone^{62,51}, J.C. Arteaga Velázquez⁶⁶, P. Assis⁷⁰, G. Avila¹¹, E. Avocone^{56,45}, A. Bakalova³¹, F. Barbato^{44,45}, A. Bartz Mocellin⁸², J.A. Bellido¹³, C. Berat³⁵, M.E. Bertaina^{62,51}, M. Bianciotto^{62,51}, P.L. Biermann^a, V. Binet⁵, K. Bismarck^{38,7}, T. Bister^{77,78}, J. Biteau^{36,i}, J. Blazek³¹, J. Blümner⁴⁰, M. Boháčová³¹, D. Boncioli^{56,45}, C. Bonifazi⁸, L. Bonneau Arbeletche²², N. Borodai⁶⁸, J. Brack^f, P.G. Brichetto Orcher^{7,40}, F.L. Briechle⁴¹, A. Bueno⁷⁵, S. Buitink¹⁵, M. Buscemi^{46,57}, M. Büskens^{38,7}, A. Bwembya^{77,78}, K.S. Caballero-Mora⁶⁵, S. Cabana-Freire⁷⁶, L. Caccianiga^{58,48}, F. Campuzano⁶, J. Caraça-Valente⁸², R. Caruso^{57,46}, A. Castellina^{53,51}, F. Catalani¹⁹, G. Cataldi⁴⁷, L. Cazon⁷⁶, M. Cerda¹⁰, B. Čermáková⁴⁰, A. Cermenati^{44,45}, J.A. Chinellato²², J. Chudoba³¹, L. Chytha³², R.W. Clay¹³, A.C. Cobos Cerutti⁶, R. Colalillo^{59,49}, R. Conceição⁷⁰, G. Consolati^{48,54}, M. Conte^{55,47}, F. Convenga^{44,45}, D. Correia dos Santos²⁷, P.J. Costa⁷⁰, C.E. Covault⁸¹, M. Cristinziani⁴³, C.S. Cruz Sanchez³, S. Dasso^{4,2}, K. Daumiller⁴⁰, B.R. Dawson¹³, R.M. de Almeida²⁷, E.-T. de Boone⁴³, B. de Errico²⁷, J. de Jesús⁷, S.J. de Jong^{77,78}, J.R.T. de Mello Neto²⁷, I. De Mitri^{44,45}, J. de Oliveira¹⁸, D. de Oliveira Franco⁴², F. de Palma^{55,47}, V. de Souza²⁰, E. De Vito^{55,47}, A. Del Popolo^{57,46}, O. Deligny³³, N. Denner³¹, L. Deval^{53,51}, A. di Matteo⁵¹, C. Dobrigkeit²², J.C. D’Olivio⁶⁷, L.M. Domingues Mendes^{16,70}, Q. Dorost⁴³, J.C. dos Anjos¹⁶, R.C. dos Anjos²⁶, J. Ebr³¹, F. Ellwanger⁴⁰, R. Engel^{38,40}, I. Epicoco^{55,47}, M. Erdmann⁴¹, A. Etchegoyen^{7,12}, C. Evoli^{44,45}, H. Falcke^{77,79,78}, G. Farrar⁸⁵, A.C. Fauth²², T. Fehler⁴³, F. Feldbusch³⁹, A. Fernandes⁷⁰, M. Fernandez¹⁴, B. Fick⁸⁴, J.M. Figueira⁷, P. Filip^{38,7}, A. Filipčič^{74,73}, T. Fitoussi⁴⁰, B. Flagg⁸⁷, T. Fodran⁷⁷, A. Franco⁴⁷, M. Freitas⁷⁰, T. Fujii^{86,h}, A. Fuster^{7,12}, C. Galea⁷⁷, B. García⁶, C. Gaudí³⁷, P.L. Ghia³³, U. Giaccari⁴⁷, F. Gobbi¹⁰, F. Gollan⁷, G. Golup¹, M. Gómez Berisso¹, P.F. Gómez Vitale¹¹, J.P. Gongora¹¹, J.M. González¹, N. González⁷, D. Góra⁶⁸, A. Gorgi^{53,51}, M. Gottowik⁴⁰, F. Guarino^{59,49}, G.P. Guedes²³, L. Gülow⁴⁰, S. Hahn³⁸, P. Hamal³¹, M.R. Hampel⁷, P. Hansen³, V.M. Harvey¹³, A. Haungs⁴⁰, T. Hebbeker⁴¹, C. Hojvat^d, J.R. Hörandel^{77,78}, P. Horvath³², M. Hrabovsky³², T. Huege^{40,15}, A. Insolia^{57,46}, P.G. Isar⁷², M. Ismaiel^{77,78}, P. Janecek³¹, V. Jilek³¹, K.-H. Kampert³⁷, B. Keilhauer⁴⁰, A. Khakurdi⁷⁷, V.V. Kizakke Covilakam^{7,40}, H.O. Klages⁴⁰, M. Kleifges³⁹, J. Köhler⁴⁰, F. Krieger⁴¹, M. Kubatova³¹, N. Kunka³⁹, B.L. Lago¹⁷, N. Langner⁴¹, N. Leal⁷, M.A. Leigui de Oliveira²⁵, Y. Lema-Capeans⁷⁶, A. Letessier-Selvon³⁴, I. Lhenry-Yvon³³, L. Lopes⁷⁰, J.P. Lundquist⁷³, M. Mallamaci^{60,46}, D. Mandat³¹, P. Mantsch^d, F.M. Mariani^{58,48}, A.G. Mariazzi³, I.C. Marić¹⁴, G. Marsella^{60,46}, D. Martello^{55,47}, S. Martinelli^{40,7}, M.A. Martins⁷⁶, H.-J. Mathes⁴⁰, J. Matthews^g, G. Matthiae^{61,50}, E. Mayotte⁸², S. Mayotte⁸², P.O. Mazur^d, G. Medina-Tanco⁶⁷, J. Meinert³⁷, D. Melo⁷, A. Menshikov³⁹, C. Merx⁴⁰, S. Michal³¹, M.I. Micheletti⁵, L. Miramonti^{58,48}, M. Mogarkar⁶⁸, S. Mollerach¹, F. Montanet³⁵, L. Morejon³⁷, K. Mulrey^{77,78}, R. Mussa⁵¹, W.M. Namasaka³⁷, S. Negi³¹, L. Nellen⁶⁷, K. Nguyen⁸⁴, G. Nicora⁹, M. Niechciol⁴³, D. Nitz⁸⁴, D. Nosek³⁰, A. Novikov⁸⁷, V. Novotny³⁰, L. Nožka³², A. Nucita^{55,47}, L.A. Núñez²⁹, J. Ochoa^{7,40}, C. Oliveira²⁰, L. Östman³¹, M. Palatka³¹, J. Pallotta⁹, S. Panja³¹, G. Parente⁷⁶, T. Paulsen³⁷, J. Pawlowsky³⁷, M. Pech³¹, J. Pěkala⁶⁸, R. Pelayo⁶⁴, V. Pelgrims¹⁴, L.A.S. Pereira²⁴, E.E. Pereira Martins^{38,7}, C. Pérez Bertolli^{7,40}, L. Perrone^{55,47}, S. Petrera^{44,45}, C. Petrucci⁵⁶, T. Pierog⁴⁰, M. Pimenta⁷⁰, M. Platino⁷, B. Pont⁷⁷, M. Pourmohammad Shahvar^{60,46}, P. Privitera⁸⁶, C. Priyatadarsi⁶⁸, M. Prouza³¹, K. Pytel⁶⁹, S. Querchfeld³⁷, J. Rautenberg³⁷, D. Ravignani⁷, J.V. Reginatto Akim²², A. Reuzki⁴¹, J. Ridky³¹, F. Riehn^{76,j}, M. Risse⁴³, V. Rizi^{56,45}, E. Rodriguez^{7,40}, G. Rodriguez Fernandez⁵⁰, J. Rodriguez Rojo¹¹, S. Rossoni⁴², M. Roth⁴⁰, E. Roulet¹, A.C. Rovero⁴, A. Saftoiu⁷¹, M. Saharan⁷⁷, F. Salamida^{56,45}, H. Salazar⁶³, G. Salina⁵⁰, P. Sampathkumar⁴⁰, N. San Martin⁸², J.D. Sanabria Gomez²⁹, F. Sánchez⁷, E.M. Santos²¹, E. Santos³¹, F. Sarazin⁸², R. Sarmento⁷⁰, R. Sato¹¹, P. Savina^{44,45}, V. Scherini^{55,47}, H. Schieler⁴⁰, M. Schimassek³³, M. Schimp³⁷, D. Schmidt⁴⁰, O. Scholten^{15,b}, H. Schoorlemmer^{77,78}, P. Schovánek³¹, F.G. Schröder^{87,40}, J. Schulte⁴¹, T. Schulz³¹, S.J. Sciutto³, M. Scornavacche⁷, A. Sedoski⁷, A. Segreto^{52,46}, S. Sehgal³⁷, S.U. Shivashankara⁷³, G. Sigl⁴², K. Simkova^{15,14}, F. Simon³⁹, R. Šmídá⁸⁶, P. Sommers^e, R. Squartini¹⁰, M. Stadelmaier^{40,48,58}, S. Stanić⁷³, J. Stasielak⁶⁸, P. Stassi³⁵, S. Strähn³⁸, M. Straub⁴¹, T. Suomijärvi³⁶, A.D. Supanitsky⁷, Z. Svozilikova³¹, K. Syrokvas³⁰, Z. Szadkowski⁶⁹, F. Tairli¹³, M. Tambone^{59,49}, A. Tapia²⁸, C. Taricco^{62,51}, C. Timmermans^{78,77}, O. Tkachenko³¹, P. Tobiska³¹, C.J. Todero Peixoto¹⁹, B. Tomé⁷⁰, A. Travaini¹⁰, P. Travnicek³¹, M. Tueros³, M. Unger⁴⁰, R. Uzeiroska³⁷, L. Vaclavek³², M. Vacula³², I. Vaiman^{44,45}, J.F. Valdés Galicia⁶⁷, L. Valore^{59,49}, P. van Dillen^{77,78}, E. Varela⁶³, V. Vašíčková³⁷, A. Vásquez-Ramírez²⁹, D. Veberič⁴⁰, I.D. Vergara Quispe³, S. Verpoest⁸⁷, V. Verzi⁵⁰, J. Vicha³¹, J. Vink⁸⁰, S. Vorobiov⁷³, J.B. Vuta³¹, C. Watanabe²⁷, A.A. Watson^c, A. Weindl⁴⁰, M. Weitz³⁷, L. Wiencke⁸², H. Wilczyński⁶⁸, B. Wundheiler⁷, B. Yue³⁷, A. Yushkov³¹, E. Zas⁷⁶, D. Zavrtanik^{73,74}, M. Zavrtanik^{74,73}

- ¹ Centro Atómico Bariloche and Instituto Balseiro (CNEA-UNCuyo-CONICET), San Carlos de Bariloche, Argentina
² Departamento de Física and Departamento de Ciencias de la Atmósfera y los Océanos, FCEyN, Universidad de Buenos Aires and CONICET, Buenos Aires, Argentina
³ IFLP, Universidad Nacional de La Plata and CONICET, La Plata, Argentina
⁴ Instituto de Astronomía y Física del Espacio (IAFE, CONICET-UBA), Buenos Aires, Argentina
⁵ Instituto de Física de Rosario (IFIR) – CONICET/U.N.R. and Facultad de Ciencias Bioquímicas y Farmacéuticas U.N.R., Rosario, Argentina
⁶ Instituto de Tecnologías en Detección y Astropartículas (CNEA, CONICET, UNSAM), and Universidad Tecnológica Nacional – Facultad Regional Mendoza (CONICET/CNEA), Mendoza, Argentina
⁷ Instituto de Tecnologías en Detección y Astropartículas (CNEA, CONICET, UNSAM), Buenos Aires, Argentina
⁸ International Center of Advanced Studies and Instituto de Ciencias Físicas, ECyT-UNSAM and CONICET, Campus Miguelete – San Martín, Buenos Aires, Argentina
⁹ Laboratorio Atmósfera – Departamento de Investigaciones en Láseres y sus Aplicaciones – UNIDEF (CITEDEF-CONICET), Argentina
¹⁰ Observatorio Pierre Auger, Malargüe, Argentina
¹¹ Observatorio Pierre Auger and Comisión Nacional de Energía Atómica, Malargüe, Argentina
¹² Universidad Tecnológica Nacional – Facultad Regional Buenos Aires, Buenos Aires, Argentina
¹³ University of Adelaide, Adelaide, S.A., Australia
¹⁴ Université Libre de Bruxelles (ULB), Brussels, Belgium
¹⁵ Vrije Universiteit Brussels, Brussels, Belgium
¹⁶ Centro Brasileiro de Pesquisas Fisicas, Rio de Janeiro, RJ, Brazil
¹⁷ Centro Federal de Educação Tecnológica Celso Suckow da Fonseca, Petropolis, Brazil
¹⁸ Instituto Federal de Educação, Ciência e Tecnologia do Rio de Janeiro (IFRJ), Brazil
¹⁹ Universidade de São Paulo, Escola de Engenharia de Lorena, Lorena, SP, Brazil
²⁰ Universidade de São Paulo, Instituto de Física de São Carlos, São Carlos, SP, Brazil
²¹ Universidade de São Paulo, Instituto de Física, São Paulo, SP, Brazil
²² Universidade Estadual de Campinas (UNICAMP), IFGW, Campinas, SP, Brazil
²³ Universidade Estadual de Feira de Santana, Feira de Santana, Brazil
²⁴ Universidade Federal de Campina Grande, Centro de Ciencias e Tecnologia, Campina Grande, Brazil
²⁵ Universidade Federal do ABC, Santo André, SP, Brazil
²⁶ Universidade Federal do Paraná, Setor Palotina, Palotina, Brazil
²⁷ Universidade Federal do Rio de Janeiro, Instituto de Física, Rio de Janeiro, RJ, Brazil
²⁸ Universidad de Medellín, Medellín, Colombia
²⁹ Universidad Industrial de Santander, Bucaramanga, Colombia
³⁰ Charles University, Faculty of Mathematics and Physics, Institute of Particle and Nuclear Physics, Prague, Czech Republic
³¹ Institute of Physics of the Czech Academy of Sciences, Prague, Czech Republic
³² Palacky University, Olomouc, Czech Republic
³³ CNRS/IN2P3, IJCLab, Université Paris-Saclay, Orsay, France
³⁴ Laboratoire de Physique Nucléaire et de Hautes Energies (LPNHE), Sorbonne Université, Université de Paris, CNRS-IN2P3, Paris, France
³⁵ Univ. Grenoble Alpes, CNRS, Grenoble Institute of Engineering Univ. Grenoble Alpes, LPSC-IN2P3, 38000 Grenoble, France
³⁶ Université Paris-Saclay, CNRS/IN2P3, IJCLab, Orsay, France
³⁷ Bergische Universität Wuppertal, Department of Physics, Wuppertal, Germany
³⁸ Karlsruhe Institute of Technology (KIT), Institute for Experimental Particle Physics, Karlsruhe, Germany
³⁹ Karlsruhe Institute of Technology (KIT), Institut für Prozessdatenverarbeitung und Elektronik, Karlsruhe, Germany
⁴⁰ Karlsruhe Institute of Technology (KIT), Institute for Astroparticle Physics, Karlsruhe, Germany
⁴¹ RWTH Aachen University, III. Physikalischs Institut A, Aachen, Germany
⁴² Universität Hamburg, II. Institut für Theoretische Physik, Hamburg, Germany
⁴³ Universität Siegen, Department Physik – Experimentelle Teilchenphysik, Siegen, Germany
⁴⁴ Gran Sasso Science Institute, L'Aquila, Italy
⁴⁵ INFN Laboratori Nazionali del Gran Sasso, Assergi (L'Aquila), Italy
⁴⁶ INFN, Sezione di Catania, Catania, Italy
⁴⁷ INFN, Sezione di Lecce, Lecce, Italy
⁴⁸ INFN, Sezione di Milano, Milano, Italy
⁴⁹ INFN, Sezione di Napoli, Napoli, Italy
⁵⁰ INFN, Sezione di Roma "Tor Vergata", Roma, Italy
⁵¹ INFN, Sezione di Torino, Torino, Italy

- ⁵² Istituto di Astrofisica Spaziale e Fisica Cosmica di Palermo (INAF), Palermo, Italy
⁵³ Osservatorio Astrofisico di Torino (INAF), Torino, Italy
⁵⁴ Politecnico di Milano, Dipartimento di Scienze e Tecnologie Aerospaziali , Milano, Italy
⁵⁵ Università del Salento, Dipartimento di Matematica e Fisica “E. De Giorgi”, Lecce, Italy
⁵⁶ Università dell’Aquila, Dipartimento di Scienze Fisiche e Chimiche, L’Aquila, Italy
⁵⁷ Università di Catania, Dipartimento di Fisica e Astronomia “Ettore Majorana“, Catania, Italy
⁵⁸ Università di Milano, Dipartimento di Fisica, Milano, Italy
⁵⁹ Università di Napoli “Federico II”, Dipartimento di Fisica “Ettore Pancini”, Napoli, Italy
⁶⁰ Università di Palermo, Dipartimento di Fisica e Chimica ”E. Segrè”, Palermo, Italy
⁶¹ Università di Roma “Tor Vergata”, Dipartimento di Fisica, Roma, Italy
⁶² Università Torino, Dipartimento di Fisica, Torino, Italy
⁶³ Benemérita Universidad Autónoma de Puebla, Puebla, México
⁶⁴ Unidad Profesional Interdisciplinaria en Ingeniería y Tecnologías Avanzadas del Instituto Politécnico Nacional (UPIITA-IPN), México, D.F., México
⁶⁵ Universidad Autónoma de Chiapas, Tuxtla Gutiérrez, Chiapas, México
⁶⁶ Universidad Michoacana de San Nicolás de Hidalgo, Morelia, Michoacán, México
⁶⁷ Universidad Nacional Autónoma de México, México, D.F., México
⁶⁸ Institute of Nuclear Physics PAN, Krakow, Poland
⁶⁹ University of Łódź, Faculty of High-Energy Astrophysics, Łódź, Poland
⁷⁰ Laboratório de Instrumentação e Física Experimental de Partículas – LIP and Instituto Superior Técnico – IST, Universidade de Lisboa – UL, Lisboa, Portugal
⁷¹ “Horia Hulubei” National Institute for Physics and Nuclear Engineering, Bucharest-Magurele, Romania
⁷² Institute of Space Science, Bucharest-Magurele, Romania
⁷³ Center for Astrophysics and Cosmology (CAC), University of Nova Gorica, Nova Gorica, Slovenia
⁷⁴ Experimental Particle Physics Department, J. Stefan Institute, Ljubljana, Slovenia
⁷⁵ Universidad de Granada and C.A.F.P.E., Granada, Spain
⁷⁶ Instituto Galego de Física de Altas Enerxías (IGFAE), Universidade de Santiago de Compostela, Santiago de Compostela, Spain
⁷⁷ IMAPP, Radboud University Nijmegen, Nijmegen, The Netherlands
⁷⁸ Nationaal Instituut voor Kernfysica en Hoge Energie Fysica (NIKHEF), Science Park, Amsterdam, The Netherlands
⁷⁹ Stichting Astronomisch Onderzoek in Nederland (ASTRON), Dwingeloo, The Netherlands
⁸⁰ Universiteit van Amsterdam, Faculty of Science, Amsterdam, The Netherlands
⁸¹ Case Western Reserve University, Cleveland, OH, USA
⁸² Colorado School of Mines, Golden, CO, USA
⁸³ Department of Physics and Astronomy, Lehman College, City University of New York, Bronx, NY, USA
⁸⁴ Michigan Technological University, Houghton, MI, USA
⁸⁵ New York University, New York, NY, USA
⁸⁶ University of Chicago, Enrico Fermi Institute, Chicago, IL, USA
⁸⁷ University of Delaware, Department of Physics and Astronomy, Bartol Research Institute, Newark, DE, USA

^a Max-Planck-Institut für Radioastronomie, Bonn, Germany^b also at Kapteyn Institute, University of Groningen, Groningen, The Netherlands^c School of Physics and Astronomy, University of Leeds, Leeds, United Kingdom^d Fermi National Accelerator Laboratory, Fermilab, Batavia, IL, USA^e Pennsylvania State University, University Park, PA, USA^f Colorado State University, Fort Collins, CO, USA^g Louisiana State University, Baton Rouge, LA, USA^h now at Graduate School of Science, Osaka Metropolitan University, Osaka, Japanⁱ Institut universitaire de France (IUF), France^j now at Technische Universität Dortmund and Ruhr-Universität Bochum, Dortmund and Bochum, Germany

Acknowledgments

The successful installation, commissioning, and operation of the Pierre Auger Observatory would not have been possible without the strong commitment and effort from the technical and administrative staff in Malargüe. We are very grateful to the following agencies and organizations for financial support:

Argentina – Comisión Nacional de Energía Atómica; Agencia Nacional de Promoción Científica y Tecnológica (ANPCyT); Consejo Nacional de Investigaciones Científicas y Técnicas (CONICET); Gobierno de la Provincia de

Mendoza; Municipalidad de Malargüe; NDM Holdings and Valle Las Leñas; in gratitude for their continuing cooperation over land access; Australia – the Australian Research Council; Belgium – Fonds de la Recherche Scientifique (FNRS); Research Foundation Flanders (FWO), Marie Curie Action of the European Union Grant No. 101107047; Brazil – Conselho Nacional de Desenvolvimento Científico e Tecnológico (CNPq); Financiadora de Estudos e Projetos (FINEP); Fundação de Amparo à Pesquisa do Estado de Rio de Janeiro (FAPERJ); São Paulo Research Foundation (FAPESP) Grants No. 2019/10151-2, No. 2010/07359-6 and No. 1999/05404-3; Ministério da Ciência, Tecnologia, Inovações e Comunicações (MCTIC); Czech Republic – GACR 24-13049S, CAS LQ100102401, MEYS LM2023032, CZ.02.1.01/0.0/0.0/16_013/0001402, CZ.02.1.01/0.0/0.0/18_046/0016010 and CZ.02.1.01/0.0/0.0/17_049/0008422 and CZ.02.01.01/00/22_008/0004632; France – Centre de Calcul IN2P3/CNRS; Centre National de la Recherche Scientifique (CNRS); Conseil Régional Ile-de-France; Département Physique Nucléaire et Corpusculaire (PNC-IN2P3/CNRS); Département Sciences de l'Univers (SDU-INSU/CNRS); Institut Lagrange de Paris (ILP) Grant No. LABEX ANR-10-LABX-63 within the Investissements d'Avenir Programme Grant No. ANR-11-IDEX-0004-02; Germany – Bundesministerium für Bildung und Forschung (BMBF); Deutsche Forschungsgemeinschaft (DFG); Finanzministerium Baden-Württemberg; Helmholtz Alliance for Astroparticle Physics (HAP); Helmholtz-Gemeinschaft Deutscher Forschungszentren (HGF); Ministerium für Kultur und Wissenschaft des Landes Nordrhein-Westfalen; Ministerium für Wissenschaft, Forschung und Kunst des Landes Baden-Württemberg; Italy – Istituto Nazionale di Fisica Nucleare (INFN); Istituto Nazionale di Astrofisica (INAF); Ministero dell'Università e della Ricerca (MUR); CETEMPS Center of Excellence; Ministero degli Affari Esteri (MAE), ICSC Centro Nazionale di Ricerca in High Performance Computing, Big Data and Quantum Computing, funded by European Union NextGenerationEU, reference code CN_00000013; México – Consejo Nacional de Ciencia y Tecnología (CONACYT) No. 167733; Universidad Nacional Autónoma de México (UNAM); PAPIIT DGAPA-UNAM; The Netherlands – Ministry of Education, Culture and Science; Netherlands Organisation for Scientific Research (NWO); Dutch national e-infrastructure with the support of SURF Cooperative; Poland – Ministry of Education and Science, grants No. DIR/WK/2018/11 and 2022/WK/12; National Science Centre, grants No. 2016/22/M/ST9/00198, 2016/23/B/ST9/01635, 2020/39/B/ST9/01398, and 2022/45/B/ST9/02163; Portugal – Portuguese national funds and FEDER funds within Programa Operacional Factores de Competitividade through Fundação para a Ciéncia e a Tecnologia (COMPETE); Romania – Ministry of Research, Innovation and Digitization, CNCS-UEFISCDI, contract no. 30N/2023 under Romanian National Core Program LAPLAS VII, grant no. PN 23 21 01 02 and project number PN-III-P1-1.1-TE-2021-0924/TE57/2022, within PNCDI III; Slovenia – Slovenian Research Agency, grants P1-0031, P1-0385, I0-0033, N1-0111; Spain – Ministerio de Ciencia e Innovación/Agenzia Estatal de Investigación (PID2019-105544GB-I00, PID2022-140510NB-I00 and RYC2019-027017-I), Xunta de Galicia (CIGUS Network of Research Centers, Consolidación 2021 GRC GI-2033, ED431C-2021/22 and ED431F-2022/15), Junta de Andalucía (SOMM17/6104/UGR and P18-FR-4314), and the European Union (Marie Skłodowska-Curie 101065027 and ERDF); USA – Department of Energy, Contracts No. DE-AC02-07CH11359, No. DE-FR02-04ER41300, No. DE-FG02-99ER41107 and No. DE-SC0011689; National Science Foundation, Grant No. 0450696, and NSF-2013199; The Grainger Foundation; Marie Curie-IRSES/EPLANET; European Particle Physics Latin American Network; and UNESCO.